

Electrical and Electroluminescent Properties of Gallium Phosphide Diffused p - n Junctions

M. GERSHENZON, R. A. LOGAN, AND D. F. NELSON
Bell Telephone Laboratories, Murray Hill, New Jersey

(Received 9 March 1966)

Reproducible properties of a large number of GaP p - n junctions made by either in-diffusion or out-diffusion of Zn were studied with emphasis on room temperature measurements. The I - V characteristics are due to space-charge recombination and are accounted for in detail by the Sah-Noyce-Shockley theory. The dominant forward-bias electroluminescence (EL) in out-diffused diodes is proven to be Zn-O acceptor-donor pair recombination at both 77 ($h\nu=1.82$ eV) and 298°K ($h\nu=1.78$ eV) from its spectral position and the shift of this position with substitution of Cd for Zn. The nonexponential time decay of this red EL in out-diffused and in-diffused diodes at 77°K also establishes it as a pair recombination mechanism. The red EL in the latter diodes at 298°K shifts anomalously in spectral position with current, thus preventing a firm identification of its mechanism at 298°K. Measurements of the spatial distribution of the red EL in all diodes show it to be generated principally in the carrier-diffusion region on the p side of the junction in a layer which saturates in brightness and then expands in width. Green EL is generated in or very near the space-charge region. By a novel use of the green EL to measure the junction bias the red EL and the I - V characteristics are studied to very high junction biases. The red EL is found to vary as $\exp(qV/mkT)$ where $m=1, 2$, and ~ 1 in successive regions. These facts, the spatial distributions, and the transition voltage between the first two regions, are in good agreement with the predictions of the preceding paper. It is shown that at the highest junction biases (~ 2.0 V) n -side injection dominates the I - V characteristic and causes a decrease in the red EL quantum efficiency. External quantum efficiencies at the optimum bias (~ 1.8 V) as high as 7×10^{-3} are found at 298°K. Several characteristics of the green and infrared EL are also given.

I. INTRODUCTION

VISIBLE light emission from forward-biased GaP diodes at room temperature has been reported by a number of investigators.¹ However, the injection mechanisms and the radiative recombination mechanisms and their interrelation were not clearly established in most cases. In many of the diodes the forward bias current was not due to thermally activated injection over a p - n junction barrier. For the diodes that were p - n junctions, the current was not explained quantitatively in terms of a dominant injection-recombination mechanism, nor were the radiative processes identified unambiguously.

The dominant current at low biases in p - n junctions made from wide band-gap semiconductors (the band gap of GaP is about 2.2 eV at room temperature) should result from thermally activated injection with recombination within the space-charge layer. The theory for this injection-recombination process has been given by Sah, Noyce, and Shockley² and, more recently, by Morgan³ with emphasis on radiative recombination.

It was recently shown from photoluminescence (PL) measurements that radiative donor-acceptor pair recombination in GaP could be fairly efficient even at room temperature when at least one level of the pair

was deep.^{4,5} In particular, pair recombination between the compensating deep donor O and the shallow acceptors Zn or Cd in p -type crystals produced broad emission bands in the red region of the spectrum (at 1.78 and 1.75 eV for the Zn-O and the Cd-O bands, respectively, at room temperature). It was shown earlier that a red emission band in GaP diodes required the simultaneous presence of Zn and O.⁶

We report here upon the room temperature electrical and electroluminescent (EL) properties of a group of over 200 GaP p - n junctions prepared by Zn or Cd diffusion into (or out of) crystals containing a shallow donor (Te) and the deep donor O. The dominant current at moderate biases will be accounted for quantitatively in terms of space-charge-layer recombination, and the dominant red EL will be shown to arise from a diffusion current on the p side of the junction. Proof that the red EL in the most efficient diodes arises from deep-donor shallow-acceptor pair (Zn-O or Cd-O) recombination at both 77 and 298°K will be presented. By a novel use of the green EL to measure the junction bias we will explore the dependence of the red EL on bias to very high biases (~ 2.0 V) and explain this dependence on a saturation of the red EL in a portion of the diffusion region which expands with increasing bias.⁷ Spatial distributions, the transient response and the occasionally observed spectral shifts of the red EL

¹ For a summary of GaP EL see for example M. Gershenzon, *Semiconductors and Semimetals, Physics of the III-V Compounds*, edited by R. K. Willardson and A. C. Beer, (Academic Press Inc., New York, 1966), Vol. II, pp. 318-325.

² C. T. Sah, R. N. Noyce, and W. Shockley, Proc. IRE 45, 1228 (1957).

³ T. N. Morgan, Phys. Rev. 139, A294 (1965).

⁴ M. Gershenzon, F. A. Trumbore, R. M. Mikulyak, and M. Kowalchik, J. Appl. Phys. 36, 1528 (1965).

⁵ M. Gershenzon, F. A. Trumbore, R. M. Mikulyak, and M. Kowalchik, J. Appl. Phys. 37, 383 (1966).

⁶ J. Starkiewicz and J. W. Allen, J. Phys. Chem. Solids 23, 881 (1962).

⁷ D. F. Nelson, preceding paper, Phys. Rev. 149, 574 (1966).

as well as some properties of the green and infrared EL will also be presented.

II. DIODE PREPARATION

A. In-Diffused Diodes

The GaP crystals used in this study were grown from Ga solutions using procedures previously described.^{4,8} For convenience, Te was selected as the *n*-type dopant since its distribution coefficient at low concentrations is ~ 15 times smaller than that of the other group VI donors (S and Se).⁹ This permitted more accurate control of the small quantities of dopant added to the melts from which the crystals were grown. The Te concentration in the melt ranged from 0.002 to 0.2 atom %; with corresponding donor concentrations of 6×10^{16} to 2×10^{18} cm⁻³ in the grown crystals.⁹ Zn was chosen as the *p*-type diffusant because of its high diffusivity.

After growth, the crystals were separated from the Ga melts by digestion in concentrated HCl. The GaP crystals thus obtained, were generally in the form of thin wafers, ~ 0.1 to 1 mm thick, with {111} major faces of dimensions ~ 3 to 8 mm in width, one side rough and one side smooth, corresponding to the P(111) face and Ga($\bar{1}\bar{1}\bar{1}$) face, respectively. Typically, one or more of the wafer edges was also planar. It was found that any plane normal to these edge faces was a cleavage plane, presumably the {110} plane. It was therefore possible to make Zn-diffused diodes with two opposite sides cleaved and parallel. This permitted optical examination of the junction EL.

The crystals used to make diodes were lapped on the rough side to a thickness of ~ 0.2 mm and visually examined for crystalline perfection. Only those crystals were selected for further processing which were single crystals and free of inclusions or other visible imperfections. The samples were briefly etched in hot aqua regia, and sealed under a vacuum of $\sim 10^{-3}$ Torr in a chemically cleaned quartz tube of volume ~ 5 cm³. The tube also contained a Zn source, separated from the samples by a quartz wool spacer. The Zn source contained some GaP to minimize surface attack on the samples. The source consisted of a mixture of 25% Zn and 75% GaP by weight which had been preheated to 1000°C for ~ 16 h in a sealed, evacuated quartz tube. The mixture was then pulverized and about 15 mg were used in each diffusion run.

The temperature of diffusion ranged from 660° to 1025°C with the sample about 10°C hotter than the Zn source and the diffusion time was selected at each temperature to provide a diffused layer of ~ 25 μ thickness except at the lowest temperatures where the

layers were 5 μ thick. After the diffusion, the samples were relapped to remove the diffused layer from the rough side. The samples were then sawed into 0.75 mm wide bars which were oriented to allow cleavage in a plane perpendicular to the sawed edges.

Ohmic contact was then made to the *p* material of the bar by the following procedure: With the sample maintained at 600°C in a vacuum of $\sim 10^{-5}$ Torr, 2000 Å of Au+0.05% Be (by weight) were evaporated through a mask to form a 0.12-mm-wide stripe on the diffused layer along the entire length of the bar. After alloying for 1 min, 500 Å of Au were deposited on the stripe with the sample maintained at 600°C and then an additional 4000 Å of Au were deposited on the stripe while the sample was slowly cooled to 200°C.

Contact to the *n*-type base material was made by plating electroless Ni onto the lapped surface for 5 min at temperatures between 90 and 93°C. Then 12000 Å of Sn were evaporated over the Ni and alloyed to the crystal at 325°C in a H₂ atmosphere.

Very light lines were then made with a diamond scribe part way across the bar at 0.6 mm intervals and the sample was cleaved into parallelepiped-shaped crystals with very light bending forces giving junctions of area $\sim 5 \times 10^{-3}$ cm². The *n* side of the wafer was then placed on a conventional Au-plated transistor header and attached by allowing the Sn contact to the header at 500°C in a H₂ atmosphere.

Contact to the *p* layer was achieved by thermo-compression bonding a Au wire to the evaporated Au stripe. Alternatively a Au wire was soldered to the stripe using a low melting solder (Pb-Sn-Bi) eutectic saturated with Au to melt at 95°C). In the latter case a surface layer that would not be readily absorbed by the solder was provided by the evaporation of 1500 Å of Ag onto the stripe while the sample was maintained at 200°C.

The series resistance associated with current flow through the diodes was generally entirely accounted for by that contributed by the bulk resistance of the *n*-type wafer. The series resistance of the contact to the diffused layer was measured as ≤ 0.09 Ω and it was assumed that the large area contact to the header was also of negligible resistance.

In most cases, the junctions were not etched after assembly. The reproducibility of the junction current-voltage (*I-V*) characteristics and the linear dependence of $\log I$ upon *V* suggested that the surface currents were negligible for $I > 10^{-8}$ A. In those cases where large leakage currents were present, normal characteristics were obtained by masking the top and cleaved surfaces of the diode with wax and etching the assembly for a few seconds in an etchant formed by flowing Cl₂ gas into a container of methyl alcohol.

A somewhat different surface condition was obtained at the junction periphery by making diodes with the usual diffusion procedures and Ohmic contacts but

⁸ J. J. Hopfield, D. G. Thomas, and M. Gershenson, Phys. Rev. Letters 10, 162 (1963); D. G. Thomas, M. Gershenson, and F. A. Trumbore, Phys. Rev. 133, A269 (1964).

⁹ F. A. Trumbore, H. G. White, M. Kowalchik, R. A. Logan, and C. L. Luke, J. Electrochem. Soc. 112, 782 (1965).

forming the junction as a mesa on the diffused surface by conventional waxing and sandblasting or etching techniques. The electrical and luminescent properties of these junctions were similar to those made with the same Zn-diffusion procedure but having sawed and cleaved sides. This suggests that surface leakage components do not contribute appreciably to the measured current at moderate to high bias. Further evidence for this is that (1) while the quantum efficiency in diodes could be varied by several orders of magnitude using different diffusion temperatures, current densities at fixed forward bias remained constant to within a factor of 5 and that (2) the reverse currents at $-2V$ bias were typically 10^{-12} A.

B. Out-Diffused Diodes

The GaP crystals used to make diodes by out-diffusion of Zn were also grown in Ga-GaP melts typically containing 0.05 atom % Zn, 0.01% Te and 0.01% Ga₂O₃. From resistivity measurements and by deducing impurity concentrations from surface-barrier-junction capacitance data, it was found that the crystals were nonuniformly doped *p* type, with a net acceptor concentration $\sim 10^{18}$ cm⁻³ on the smooth $\{\bar{1}\bar{1}\bar{1}\}$ side and 10^{17} cm⁻³ on the opposite rough face.

p-n junctions were readily formed within a few microns of the smooth $\{\bar{1}\bar{1}\bar{1}\}$ face by out-diffusion of Zn forming an *n* layer due to the residual compensating Te donors. This was accomplished by heating the samples for a few minutes at 600°C. Thus the heat-treatments employed to make the Ohmic contacts were sufficient to develop the junctions. The Au-Be contact to the *p* side was the same as that used to the Zn-diffused layer of in-diffused diodes. An adequate contact to the *n* layer was formed by evaporation of a Au or Sn film onto the sample held at 600°C to permit alloying. Both cleaved- and mesa-type structures were made from the out-diffused junctions. With similar fabrication procedures, out-diffused diodes were also prepared from crystals grown from melts in which the Zn was replaced by 7 atom % Cd.

III. ELECTRICAL PROPERTIES

A. Theory

The dependence of space-charge recombination current on bias was derived by Sah, Noyce, and Shockley (SNS)² and applied to radiative space-charge recombination by Morgan.³ Following SNS we can estimate the ratio of the space-charge current density (J_s) to the diffusion current density (J_d) by assuming that a single level at the intrinsic Fermi level dominates the recombination both in the space-charge layer and beyond, with equal electron- and hole-capture cross sections and with identical free carrier densities and mobilities on either side of the step junction. Using a carrier density of 10^{18} cm⁻³, a diffusion length of 10^{-4}

cm and a space-charge width of 10^{-5} cm, we find that $J_s/J_d \sim 10^3$ at 1.5 V, the lowest bias at which the leakage currents can be neglected, and $J_s=J_d$ at ~ 1.85 V, roughly the highest bias before series resistance dominates the *I-V* curves. Therefore recombination in the space-charge layer will dominate in the accessible voltage range.

SNS showed that the quasi-Fermi levels remain constant throughout the space-charge layer up to moderate biases and also that a linearly varying junction potential is a good approximation. Under these conditions the space-charge recombination currents through each recombination center and the diffusion currents on both the *n* and the *p* sides of the junction are all parallel independent processes, each driven by the same applied potential *V*.

For $eV/2kT > 1$ the SNS expression for the space charge current density through one recombination center is

$$J_s = \frac{n_i k T W \exp(qV/2kT)}{[\tau_{p0}\tau_{n0}]^{1/2}(V_d - V)} f(b), \quad (1)$$

where n_i is the intrinsic carrier density, W is the junction width (dependent on V), V_d is the built-in potential, and τ_{p0} (τ_{n0}) is the hole (electron) lifetime associated with the center when it is filled with electrons (holes). $f(b)$ is a definite integral given by SNS and b is given by

$$b = \cosh[(E - E_i)/kT] + \ln(\tau_{p0}/\tau_{n0})^{1/2} \exp(-qV/2kT), \quad (2)$$

where E is the energy of the level and E_i is the energy of the intrinsic Fermi level (positive toward the valence band).

For $b \ll 1$ (high bias) and $(V_d - V) \gg kT$, $f(b) \approx \pi/2$ and therefore

$$J_s \sim [W/(V_d - V)] \exp(qV/2kT). \quad (3)$$

For $b \gg 1$ (low bias) and $(V_d - V) \gg kT$, $f(b) \approx b^{-1} \ln b$, and so

$$J_s \sim \left[\left| \frac{E - E_i}{kT} + \frac{1}{2} \ln \frac{\tau_{p0}}{\tau_{n0}} \right| + \ln \frac{1}{2} - \frac{qV}{2kT} \right] \frac{W}{2kT} \exp(qV/kT). \quad (4)$$

The transition between these two regions occurs when $b=1$ or when the bias is

$$V_k = \left| \frac{2(E - E_i)}{q} + \frac{kT}{q} \ln \left(\frac{\tau_{p0}}{\tau_{n0}} \right) \right| + \frac{2kT}{q} \ln \frac{1}{2}. \quad (5)$$

For $V > V_k$, $J_s \sim \exp(qV/nkT)$ with $n=2$. However, the pre-exponential factor (W varying less rapidly with V than does $V_d - V$) increases the slope, so that the

TABLE I. Diode classification based upon $I-V$ and capacitance-voltage behavior shown together with the modes of preparation.

Class	Type of diffusion	Diffusion temperature (°C)	Diffusion time (h)	Profile	Capacitance i layer	Recombination implied by $I-V$ characteristic
A	In-diffusion	660	17-60	Step	No	Deep level
		735	17-60			
		825	<4			
B	In-diffusion	725	>100	Step	Yes	Deep level
		825	17			
C	In-diffusion	825	17	Graded	No	Deep and shallow levels
		1025	0.5			
D	Out-diffusion	600		Graded	Sometimes	Shallow levels

measured n will be somewhat less than 2. For $V < V_k$, $n=1$, but this time the pre-exponential factor tends to decrease the current so that the measured n will be somewhat greater than 1. Note that (with $\tau_{p0} \approx \tau_{n0}$) for a deep level near the center of the gap, $E=0$, $V_k=0$, and only the high bias behavior can be observed, whereas for a very shallow level, $E \approx \frac{1}{2}E_g$, $V_k = E_g/q$ and only the low bias case can be observed. (E_g is the band gap.)

B. Experimental Results

The relationships between current and voltage and between capacitance and voltage as determined on about 200 diodes form the basis for classifying the diodes into four groups as indicated in Table I. The first group (class A) consists of in-diffused diodes prepared by low temperature diffusions. Class B contains those made by diffusions for longer periods of time or at higher temperatures. In class C are diodes diffused at the highest temperatures. Class D consists of the out-diffused structures.

The dependence of junction capacitance upon bias is shown in Fig. 1 for a typical diode from each class. The class-A diodes are simple step junctions with C^{-2} varying linearly with bias. The class-B diodes are also step junctions but an i layer of approximately one half of the junction width at zero bias must be invoked to account for the abnormally large extrapolated intercept on the voltage axis.¹⁰ The presence of the i layer was also indicated by comparing the electric field dependence of the carrier ionization rates in avalanche multiplication in these junctions with those without i layers.¹¹ The class-C diodes are simple linearly graded junctions and the class-D diodes are also linearly graded, but usually with an i layer present. The junction widths at zero bias ranged between 500 and 3000 Å and the built-in potentials in the absence of i layers were 2.0 ± 0.1 V. The departures of the experimental points from the power law curves in forward bias are attributed to the presence of deep impurity states.¹²

¹⁰ R. A. Logan and A. G. Chynoweth, J. Appl. Phys. **33**, 1649 (1962).

¹¹ R. A. Logan and H. G. White, J. Appl. Phys. **35**, 3945 (1965).

¹² T. N. Morgan, IEEE Trans. Electron Devices **ED-11**, 533 (1964).

The diode current is plotted logarithmically against forward bias at room temperature in Fig. 2 for a typical diode from each class. Such curves can usually be approximated by several straight lines in the bias range covered, implying that the current I is related to the voltage V by $I = I_0 \exp(AV)$, with the empirical constant A different in each region. Thermal injection

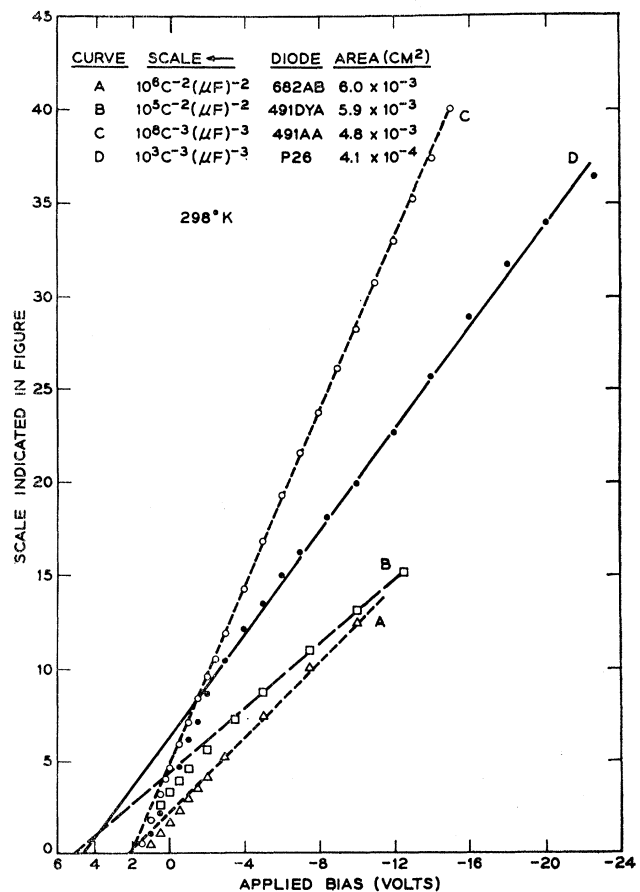


FIG. 1. The dependence of the capacitance upon the applied bias for a representative diode of each diode class. The examples of classes A and B are step junctions and those of classes C and D are linearly graded junctions. In addition, the class-B and class-D diodes contain i layers.

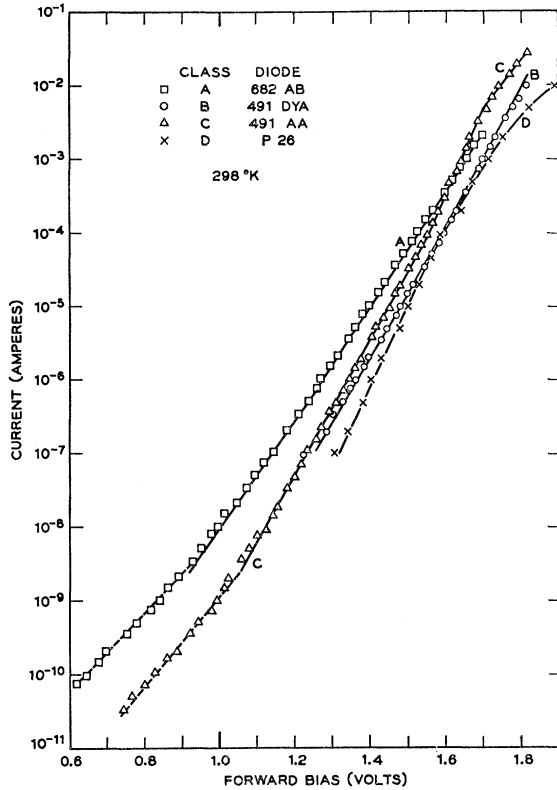


FIG. 2. Forward-bias I - V curves for the representative diodes of Fig. 1. The dashed portions of the curves at the lowest biases are due to leakage currents. At high biases the curves are truncated before the series resistance becomes large. Series resistance corrections are not shown.

currents are expected to vary as $\exp(qV/nkT)$, where q is the electronic charge, T is the temperature, k is Boltzmann's constant, and n a parameter ($1 \leq n \leq 2$) in each region that is independent of temperature.^{2,13} Figure 3 shows the I - V relationship at several temperatures of an out-diffused diode for which n is a constant (1.5) throughout the voltage and temperature ranges studied.

The apparent increase of n to values greater than two in the low current region of Fig. 2 is due to an excess current. In this region n cannot, in fact, be defined since it would have to be temperature dependent. This excess current was found to increase with time and to be altered by thermal cycling or surface treatment. Hence it is believed to be a surface current and will not be considered further.

At high bias the current is limited by series resistance in the diodes of Fig. 2. The series resistance in these diodes varied between 0.2 and 20 Ω at room temperature, the higher values corresponding to the out-diffused diodes. The magnitude of the resistance and its temperature dependence could be accounted for by considering the geometry and the doping of the bulk

n side of the in-diffused diodes and the p side of the out-diffused diodes.

The mean minority carrier lifetime, $\tau_m = [(b\tau_n)^{1/2} + \tau_p^{1/2}]^2$, where b is here the electron-to-hole mobility ratio, was estimated by techniques described elsewhere.¹⁰ In the diodes studied, τ_m ranged from 1×10^{-8} to 4×10^{-10} sec and in general did not correlate with the efficiency or other diode properties. However, as noted previously,¹⁴ for diodes made by Zn diffusion at a fixed temperature into crystals grown from the same melt, τ_m scaled with the quantum efficiency.

C. Comparison with Theory

In the past, space-charge recombination has been implicated qualitatively when the measured parameter n lay between 1 and 2. We wish to show that the I - V curves of most of the GaP diodes can be fit quantitatively by the SNS theory with deep-level recombination dominating in the class-B diodes, shallow-level recombination in the class-D diodes, and both deep level and shallow-level recombination in the class-C diodes. The class-A diodes can be fit only if the width of the junction varies anomalously with bias, an effect which has support from the capacitance versus voltage data.

We shall assume in the moderate forward bias range of interest ($1.6 \text{ V} < V < 1.8 \text{ V}$) that (1) although direct capacitance measurements are not possible owing to the low junction impedance, the width of the space-charge layer continues decreasing at the same rate as it does with decreasing reverse bias and (2) for the diodes with built-in intrinsic layers where the junction

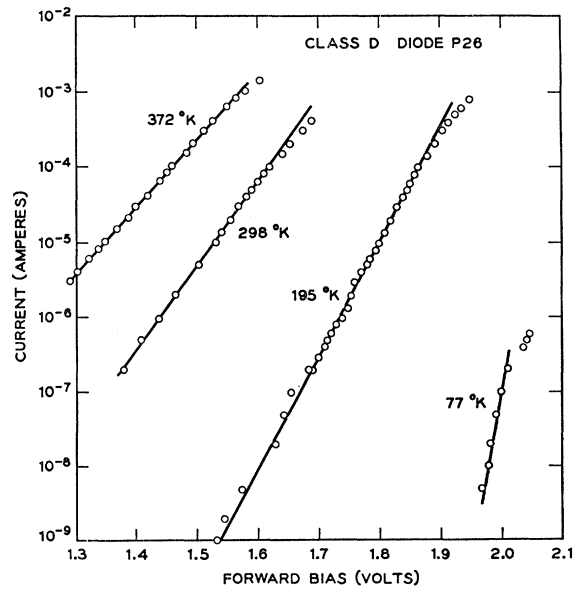


FIG. 3. I - V curves for a class-D diode at several temperatures with no series-resistance corrections at the highest biases. The straight lines correspond to a slope of $q/1.50kT$ at all temperatures.

¹³ W. Shockley, Bell System Tech. J. 28, 435 (1949).

¹⁴ R. A. Logan, H. G. White, and R. M. Mikulyak, Appl. Phys. Letters 5, 41 (1964).

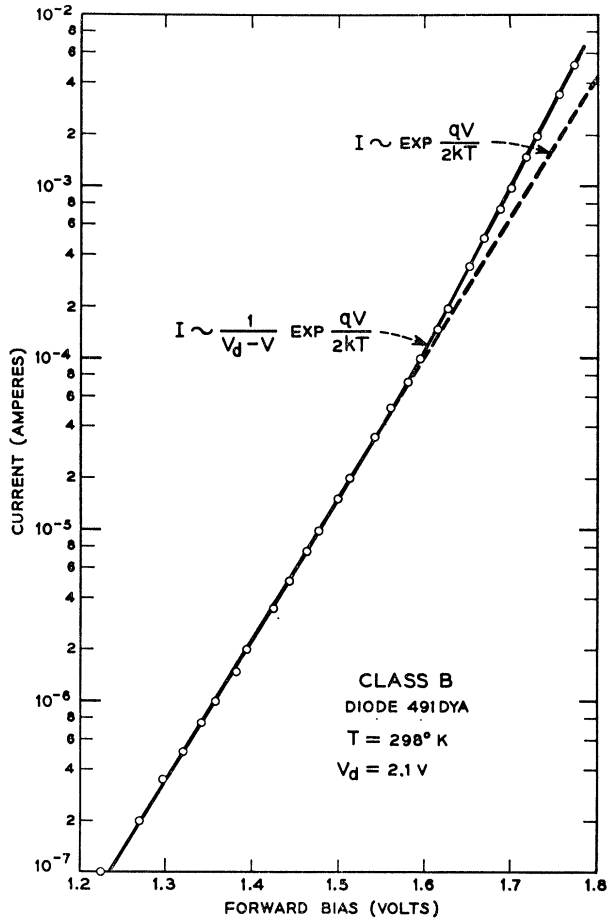


FIG. 4. The I - V curve for a class-B diode. The dashed curve corresponds to a $\exp(qV/2kT)$ dependence of current upon bias which is a good approximation at low bias. The solid curve represents the fit from the SNS theory for deep-level space-charge recombination. The region where series resistance becomes important is not shown.

width becomes comparable to that of the intrinsic layer, the space-charge layer width is constant and is equal to that of the intrinsic layer. The validity of these assumptions will be discussed later. It is also noted that even at the highest biases studied, $(V_d - V)$ is still much greater than kT so that the I - V characteristic may be compared to SNS theory.

For all the class-B diodes n is equal to 2 for biases just above the leakage current range but as the applied potential approaches V_d , n decreases, as evident in Fig. 4. This is the expected result for the case of a deep recombination level and $V > V_k$. The class-B diodes possess i layers and so we assume that W is independent of bias in the bias range of Fig. 4. V_d is determined from capacitance data. Therefore the unknown proportionality constant of Eq. (3) is obtained by fitting to the data at low biases. This is shown in Fig. 4. If W had been allowed to vary with bias, the fit would not have been as good.

Since $V > V_k$ over the entire bias range, we can use Eq. (5) to obtain limits on E for the dominant recombination level. If $\tau_{p0} = \tau_{n0}$ the level must lie at least 0.47 eV from either the conduction or the valence band, and with $\tau_{p0}/\tau_{n0} = 10^{-4}$ for an acceptor or 10^{+4} for a donor, the level must lie at least 0.36 eV from the appropriate band edge. By fitting the one unknown parameter from Eq. (1) we obtain $(\tau^*)^{-1} \equiv \sum (\tau_{p0}\tau_{n0})^{-1/2}$, the summation being over all levels which contribute to the current. The fit shown in Fig. 4 yields $\tau^* \sim 10^{-11}$ sec, which within a factor of 10 is characteristic of all the class-B diodes.

The I - V characteristics of class-C diodes, like the class-B diodes, have $n = 2$ at low bias but they exhibit two kinks (corresponding to decreases in n) at higher applied potentials (see Fig. 2). These curves cannot be fit over their entire range by assuming $V > V_k$, no matter which simple bias dependence is taken for W . The data can be fit, however, by assuming a deep level ($V > V_k$) giving rise to the $n = 2$ region at low bias and an additional relatively shallow level producing the kinks (and the excess current) at the higher biases.

The class-C diodes are linearly graded junctions with no i layers and we assume for now that the junction

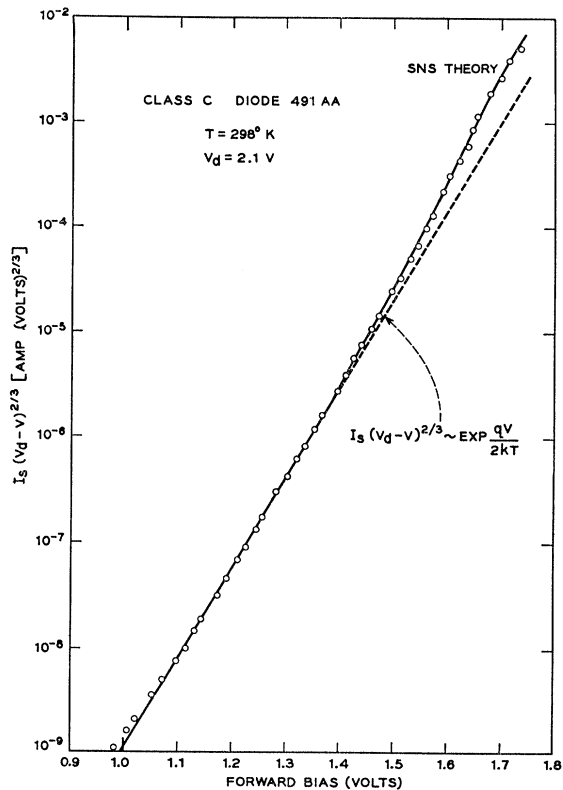


FIG. 5. The bias dependence of the current (I_s) multiplied by $(V_d - V)^{2/3}$ for a class-C diode. The dashed line represents the current due to space-charge recombination at a deep level and the solid line is the sum of both deep-level and shallow-level recombination, the latter determined from a fit to $f(b)$ as described in the text.

width continues to decrease with bias as $(V_d - V)^{1/3}$. Then if we multiply both sides of Eq. (1) by $(V_d - V)^{2/3}$ we obtain

$$J_s(V_d - V)^{2/3} = \lambda \sum_j (\tau_{p0}\tau_{n0})_j^{-1/2} \times \exp(qV/2kT) f(b_j), \quad (6)$$

where the summation is over each recombination level that contributes to the current and $\lambda = n_i k T W_0 V_d^{-1/3}$, W_0 being the junction width at zero bias. In Fig. 5 we multiply the current by $(V_d - V)^{2/3}$ (V_d obtained from the capacitance data) and plot the logarithm of the product against V . The fit to the lower $n=2$ range (assuming $V > V_k$) determines the unknown proportionality constant as before. Both the limits on the depths of the contributing levels and τ^* are found to be identical to their values for the class B diodes. Next, this ($n=2$) current component is subtracted from the total current. We attribute the remaining current to recombination at a relatively shallow level where V may be of order of V_k . This remainder, now treated as an independent space-charge recombination current, is then multiplied by $\exp(-qV/2kT)$ and compared to

$$K_{sj} = J_{sj}(V_d - V)^{2/3} \exp(-qV/2kT) = \mu_j f(b_j), \quad (7)$$

where $\mu_j = \lambda(\tau_{p0}\tau_{n0})_j^{-1/2}$ and j refers to the shallow recombination level.

We can rewrite Eq. (2) for the case where the hyperbolic cosine can be replaced by $\frac{1}{2}$ the exponential as

$$b = \exp[q(V_k - V)/2kT]. \quad (8)$$

Thus if we plot $\log K_{sj}$ against V , we may compare the result with $f(b)$ as given by SNS. In this case we have two parameters at our disposal, V_k , the additive constant for the voltage scale, and $\log \mu$, the additive constant on the $\log K_{sj}$ scale. From this fit, which encompasses the range on both sides of V_k , we obtain both V_k and μ for the shallow level. From the fitted value of V_k (1.65 V) we deduce that the level lies 0.25 eV from one of the band edges if $\tau_{p0}/\tau_{n0} = 1$ or 0.14 eV from the edge of the valence (conduction) band if the center is an acceptor (donor) with $\tau_{p0}/\tau_{n0} = 10^{-4}$ (10^4). These values are somewhat greater than the binding energies of the shallow levels known to be present (Te: 0.11¹⁵ or 0.08 eV,¹⁶ Zn: 0.05 eV¹⁷).

From the fitted value for μ we deduce that $(\tau_{p0}\tau_{n0})^{1/2} \sim 10^{-10}$ sec. Again if $\tau_{p0}/\tau_{n0} = 10^{-4}$ (shallow acceptor), then $\tau_{p0} \sim 10^{-12}$ sec and $\tau_{n0} \sim 10^{-8}$ sec (and *vis-à-vis* for a shallow donor).

The values of V_k and μ so determined are used with $f(b)$ and Eqs. (6), (7), and (8) to synthesize the total junction current as a sum of its two components, and this curve is also shown in Fig. 5. In this case the fit

would be equally good if W were proportional to $(V_d - V)^m$ with $0 < m < 0.5$.

For the class-D out-diffused diodes, only a more limited bias range could be measured because of greater series resistance and higher leakage currents. They can be fitted approximately by shallow-level recombination with V_k very close to that for the class-C diodes. The shortness of the measurement range prohibits determining the characteristics of any deep-level recombination.

The ability to fit the I - V characteristic to SNS theory critically depends upon the variation of junction width with bias through the term $W/(V_d - V)$ in Eq. (1). The class-A diode characteristics are inconsistent with SNS theory if one assumes $W \propto (V_d - V)^{1/2}$ as inferred by the reverse bias capacitance measurements but would agree with theory if $W \propto (V_d - V)$. In forward bias ($0 < V < 1.65$ V) the measured capacitance is larger than that obtained by extrapolation of the reverse bias data (see Fig. 1), an effect ascribed to the presence of deep states.¹² The measured capacitance thus increases more rapidly than that for a step junction. This effect would reconcile the I - V characteristic with SNS theory if it persisted into the voltage range of interest, 1.6 V $< V < 1.8$ V, where direct capacitance measurements are not possible owing to the low junction resistance ($R \lesssim 25 \Omega$).

Since the class-C diodes are fit to SNS theory by an addition of independent components, the fit is less sensitive to the assumed bias dependence of W and good agreement is obtained with $W \propto (V_d - V)^m$ where $0 < m \leq 0.5$. Thus, just as for the class-A diodes, it is possible to fit the characteristics to SNS theory with a width which decreases more rapidly with forward bias than with reverse bias [$W \propto (V_d - V)^{1/3}$ for the class-C diodes].

The class-B and -D diodes contain an i layer of width $W_I \leq 0.5W_0$. In the bias range $1.6 \leq V \leq 1.8$ V, where the junction width variation influences the comparison of the characteristics to SNS theory, $W_I \leq W < 1.2 W_I$ and changes $\leq 10\%$ with bias, so that to a good approximation W may be set constant and equal to W_I as done above.

Above ~ 1.8 V, where series resistance prevents direct measurement of the junction voltage, the I - V characteristic can be deduced from a plot of the green EL intensity versus current (see Sections VB and VD and Fig. 19). It will be shown in Section VD that diffusion current dominates the I - V characteristic at the highest biases, as expected.

IV. RADIATIVE RECOMBINATION MECHANISMS

A. Experimental Technique

Spectra were obtained both with dc current excitation and with pulsed excitation with the diodes immersed in silicone oil (to assist in heat dissipation) contained in a Dewar so that by heating the oil or cooling it with dry ice, spectra could be obtained between 200 and

¹⁵ D. N. Nasedov, V. V. Negreskul, and S. V. Slobodchikov, *Fiz. Tverd. Tela* **7**, 1912 (1965) [English transl.: *Soviet Phys.—Solid State* **7**, 1549 (1965)].

¹⁶ H. C. Montgomery and W. L. Feldmann, *J. Appl. Phys.* **36**, 3228 (1965).

¹⁷ M. Gershenzon (unpublished).

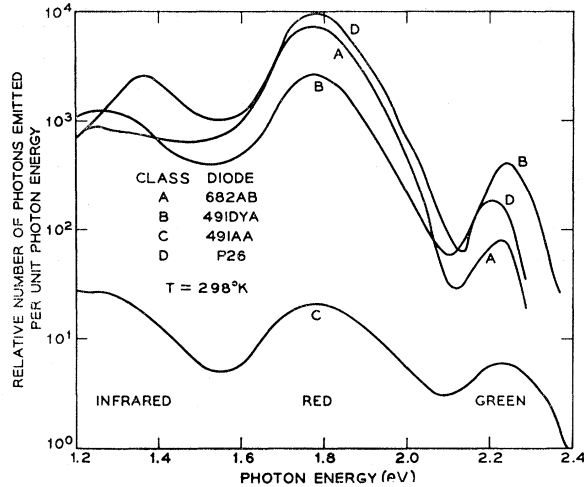


FIG. 6. Forward-bias EL spectra of the representative diodes of each class for which the bias dependence of capacitance (Fig. 1) and current (Fig. 2) have already been shown. All spectra shown here were obtained at 5 mA dc and are shown approximately normalized to each other (however, the junction areas vary, see Fig. 1). The green band for the class-C diode is the only peak here that is resolution-limited.

400°K. In addition, some diodes were immersed directly in liquid N_2 to extend the range to 77°K. A Perkin-Elmer double-pass quartz prism monochromator was used for the dc experiments (10^{-6} – 10^{-2} A) utilizing both photomultipliers (RCA 7326 and 7102) and a PbS cell as detectors. For high level excitation the diodes were driven with 0.5 μ sec pulses, the applied voltage being limited by surface breakdown at ~ 30 000 V/cm across a cleaved junction surface and somewhat lower than this for the mesa diodes. Pulsed currents ranged from 10^{-3} to 20 A. A Perkin-Elmer grating monochromator (without the chopper) was used to disperse the light which was detected by a cooled photomultiplier (RCA 7326) and displayed on a Hewlett-Packard 185B sampling oscilloscope using a 1 μ sec RC time constant at the input to minimize photon noise arising from the short sampling time (0.5 nsec) of the oscilloscope. The dc output of the oscilloscope was fed to a strip-chart recorder whose drive was synchronized with the wavelength drive of the monochromator. After correcting for the wavelength response of the system, the spectra were plotted in terms of the relative number of photons emitted per unit energy increment as a function of photon energy in eV.

B. Spectra

The forward-bias room-temperature EL spectrum of a representative diode from each class is shown in Fig. 6. Three EL bands are apparent, one in the green (2.2 eV), one in the red (1.8 eV) and one or more in the near infrared (~ 1.3 eV). These bands appear throughout the temperature range investigated, 77–400°K. The integrated strength of the red band was almost always stronger than either of the other two emission bands.

C. Red Band

We will now show that the red EL emission which peaks at 1.78 eV with a half-width of 0.19 eV at 298°K is a donor-acceptor pair transition between a shallow Zn acceptor and a deep O donor. We do this by comparing the diode spectra with spectra of homogeneous *p*-type samples containing both Zn and O. Comparison to *p*-type crystals is appropriate since we will show in a later section that the red EL is generated predominantly on the *p* side of the junctions. As will be described later, the red peak in the in-diffused diodes shifts with bias at 298°K but the spectral position in the more efficient out-diffused junctions is independent of bias. We thus start by comparing the latter class with PL data.^{4,5}

In homogeneous *p*-type samples doped with the acceptor Zn and somewhat compensated by the donor O, the red PL emission was shown to be due to donor-acceptor pair emission involving Zn and O.^{4,5,18} Measurement of the spectral shift of the red band with change of the acceptor from Zn to Cd, one of the methods used to identify the pair band mechanism in PL, can be used to establish the mechanism in EL.

Figure 7 shows the position of the PL peak at 77°K as a function of the excitation intensity in a Zn-O

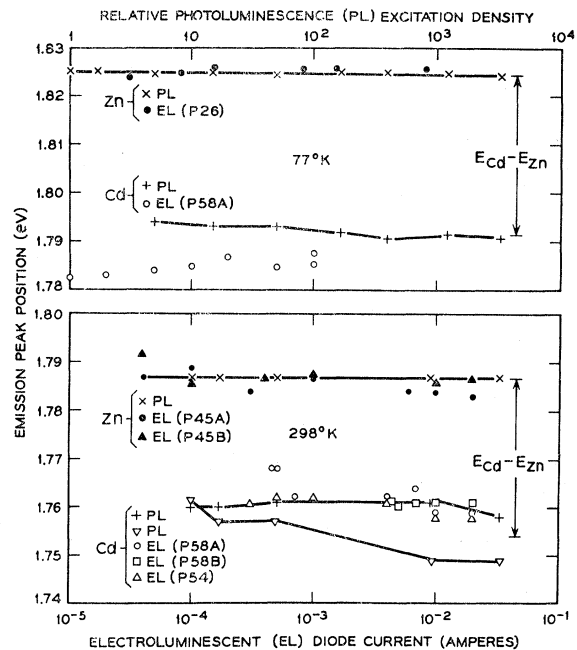


FIG. 7. The spectral positions of the red PL band at both 77 and 298°K in samples doped with optimum concentrations (Refs. 4 and 5) of Zn and O, or Cd and O, as a function of the intensity of PL excitation and the spectral positions of the red EL band in out-diffused diodes (class D) containing Zn and O, or Cd and O, as a function of the forward bias current. The marked intervals show the difference in acceptor binding energy between Cd and Zn (Ref. 19).

¹⁸ D. F. Nelson and K. F. Rodgers, Phys. Rev. **140**, A1667 (1965).

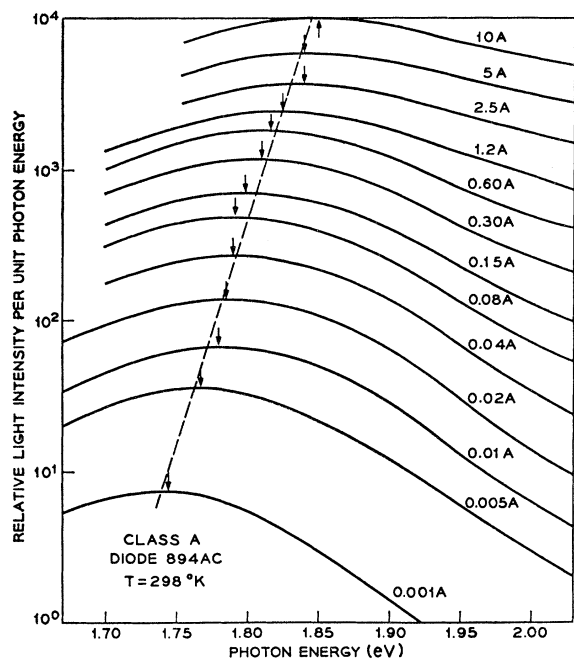


FIG. 8. The spectral intensity of the red EL from an in-diffused diode for several current excitation values. The lowest two curves were obtained with dc excitation; the others with 0.5- μ sec current pulses. The peak position (shown by an arrow) shifts by 0.105 eV in this diode.

compensated *p*-type sample.⁴ Also shown are similar data for a sample where Cd has been substituted for Zn.⁴ The positions of both bands are independent of excitation intensity but the Cd-O band has been shifted to lower energies relative to the Zn-O band by 0.033 eV which is the difference in binding energies between Cd and Zn.¹⁹ Figure 7 also shows the positions of the red EL band as a function of current at 77°K in two out-diffused diodes, one containing Zn and O and the other with Cd in place of Zn. The EL peaks do not shift with current, and their agreement with the positions of the PL bands shows that the red EL at 77°K emitted by the diodes in forward bias is a donor-acceptor pair band involving both Zn (or Cd) and O as acceptor and donor, respectively. The scatter of points in Fig. 7 is reasonable in view of the width of the emission band (0.15 eV at 77°K and 0.19 eV at 298°K). If the emission were due to radiative capture of a free hole by a neutral O donor, there would be no difference in the spectra of the Zn and the Cd-doped samples.

PL results indicate that the Zn-O pair band is still the dominant radiative recombination mechanism at room temperature in samples containing optimum concentrations of both Zn and O,⁵ with external quantum efficiencies as high as 11%.²⁰ The Zn acceptor in these *p*-type crystals is deep enough (0.05 eV) so that even

at 298°K a significant number of majority carrier holes remain frozen out on the Zn acceptors at thermal equilibrium.⁵ Injected minority carriers (electrons), are captured efficiently by the positively charged compensating O donors, and because these donors are so deep (~ 0.4 eV), thermal ionization of the trapped carriers is still small enough to permit efficient emission at 298°K.

Figure 7 compares the spectral positions of the red emission bands as a function of excitation intensity at room temperature from PL (Zn-O- and Cd-O-doped samples) with those from EL (Zn-Te-O- and Cd-Te-O-doped out-diffused diodes). Again the peaks do not shift with excitation but do exhibit the Zn-Cd shift. Therefore, these bands are still dominantly pair bands even at room temperature.

The spectral positions of these peaks in out-diffused diodes do not follow the temperature variation of the band gap but are ~ 0.07 eV higher in energy at 298°K relative to the band gap than they were at 77°K. This is reasonable because thermal ionization at the higher temperatures removes carriers from the distant (slow) pairs and allows them to recombine at closer (faster) pairs. At 77°K the average pair separation (at the peak of the emission) is ~ 50 Å,⁴ whereas at 298°K a shift of 0.07 eV implies an average separation of ~ 15 Å. This effect supports the pair-band interpretation.

The spectral position of the red EL in the in-diffused diodes at 77°K is usually close to that expected (see Fig. 7) for the Zn-O pair band. The peak position in some diodes, however, can be 0.01 eV low. The firmest evidence that the red EL in the in-diffused diodes results from donor-acceptor pair recombination is that its time decay at 77°K is nonexponential. This result is similar to the decay of the Zn-O band in PL at 77°K.¹⁸ The EL decay can be measured for nearly a second and it approximates a t^{-1} dependence. Similar results have been obtained for out-diffused diodes at 77°K. Rapid thermal ionization prevents similar measurements at room temperature as it does in PL also.

The identification of the red EL at 298°K in in-diffused diodes, in contrast to the out-diffused diodes, is complicated by its shift in frequency as the current is changed. Figure 8 illustrates this effect. The photon energy $h\nu_p$ of the peak intensity is seen to shift with light intensity L as $h\nu_p = E_0 \ln L + \text{const}$, where $E_0 = 0.0146$ eV for this diode. Since E_0 has been found to vary from diode to diode between 0.006 and 0.026 eV, a comparison of the spectral positions of the red EL from Zn and Cd in-diffused diodes cannot be used to identify the red EL as a pair band at 298°K.

Though the origin of this spectral shift is not presently understood, the following observations limit the problem somewhat. As will be shown in Sec. VA for both in-diffused and out-diffused diodes, the red EL is generated in a layer on the *p* side of the junction which expands further into the *p* material at higher currents. For the out-diffused diodes, for which there

¹⁹ F. A. Trumbore and D. G. Thomas, Phys. Rev. **137**, A1030 (1965).

²⁰ M. Gershenzon and R. M. Mikulyak, Appl. Phys. Letters **8**, 245 (1966).

is no spectral shift, the *p* side is homogeneously doped material. For the in-diffused diodes, with which the spectral shift is observed, the *p* side consists of a Zn diffusion profile. Thus, higher emission frequencies correlate with emission from more heavily Zn-doped material. A further characteristic of the spectral shift, already noted, is that it disappears at 77°K. However, since the higher series resistance of the diodes at 77°K limits the current range that can be studied, we can say only that E_0 at 77°K is at least four times smaller than at 298°K.

D. Green Band

In the past several emission mechanisms giving green PL have been positively identified at low temperature where the spectra contain many sharp line components. These include excitons bound to an un-ionized donor (S),²¹ excitons bound to isoelectronic traps (N atoms substituted for P atoms, or pairs of the same),²² and shallow-donor shallow-acceptor pair recombination.^{8,19} These peaks have also been observed in EL at low temperatures.²³ The breadth of the green bands at room temperature has so far prevented such conclusive identification. Band-to-band,^{24,25} free-to-bound,^{26,27} pair,²⁸ and isoelectronic trap (the "A line")^{23,28} recombination have been suggested.

All of the diodes studied here have emitted green EL near 2.2 eV at room temperature at least at high excitation levels. Figure 6 shows representative spectra. Since the emphasis of this work has been on the dominant red EL for which self-absorption is unimportant, no care to avoid self-absorption of the luminescence was taken. Because of intrinsic absorption, self-absorption of the green EL is clearly important, particularly for the in-diffused diodes for which the green peak lies above its position indicated in Fig. 6. If the band gap is taken as 2.20 eV,²⁹ this is substantial evidence that the band-to-band process is being observed in in-diffused diodes. However, recent absorption measurements³⁰ indicate a band gap at room temperature some 0.06 eV higher than previously believed.²⁹ Since intrinsic emission can be as much as 0.05 eV

²¹ D. G. Thomas, M. Gershenson, and J. J. Hopfield, Phys. Rev. **131**, 2397 (1963).

²² D. G. Thomas, J. J. Hopfield, and C. J. Frosch, Phys. Rev. Letters **15**, 857 (1965).

²³ M. Gershenson, R. M. Mikulyak, R. A. Logan, and P. W. Foy, Solid-State Elect. **7**, 113 (1964).

²⁴ E. E. Loebner and E. W. Poor, Phys. Rev. Letters **3**, 23 (1959).

²⁵ M. Gershenson and R. M. Mikulyak, J. Appl. Phys. **32**, 1338 (1961).

²⁶ J. W. Allen, M. E. Moncaster and J. Starkiewicz, Solid-State Electron. **6**, 95 (1963).

²⁷ H. G. Grimmeiss and H. Koelmans, Phys. Rev. **123**, 1939 (1961); H. G. Grimmeiss, A. Rabenau, and H. Koelmans, J. Appl. Phys. **32**, 2123 (1961).

²⁸ L. M. Foster and M. Pilkuhn, Appl. Phys. Letters **7**, 65 (1965).

²⁹ W. G. Spitzer, M. Gershenson, C. J. Frosch, and D. F. Gibbs, J. Phys. Chem. Solids **11**, 339 (1959).

³⁰ P. J. Dean (private communication).

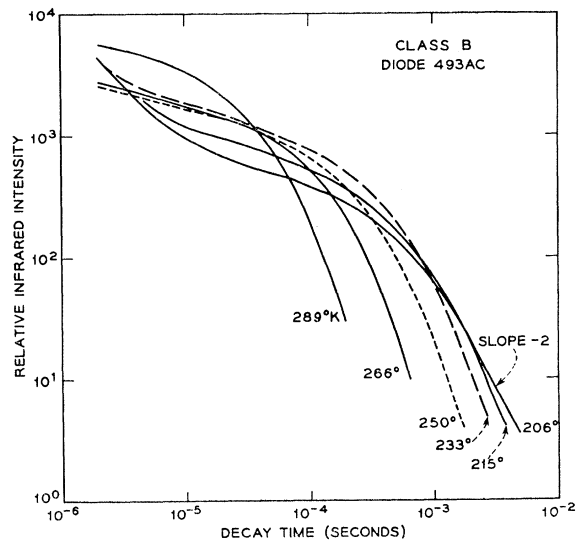


FIG. 9. The nonexponential time decay of the infrared EL at several temperatures.

below the energy gap because of phonon emission, the green band may still be intrinsic but the involvement of a shallow defect level cannot be excluded at present.

The spectral position of the green peak from out-diffused diodes, in general, is lower than that from in-diffused diodes. This does not appear to be a self-absorption effect from a comparison of geometries. Further, for the out-diffused diodes the origin of the green emission was shown to be the space-charge layer at moderate biases (see Sec. VA). On the basis of its origin and its efficiency the following argument shows that the green EL cannot result from band-to-band recombination. The band-to-band recombination rate per unit junction area is $U = WBpn = WBn_i^2 \times \exp(qV/kT)$, where W is the width of the space-charge layer and B is the recombination constant for band-to-band recombination. B can be obtained from absorption edge data by a detailed balance argument to be $\sim 10^{-15}$ cm²/sec. The quantum efficiency for band-to-band recombination is then qU/J , where J is the measured current density corresponding to V . With $n_i = 1.4$ cm⁻³ and $W = 10^{-5}$ cm the calculated quantum efficiencies are 10^8 to 10^6 times smaller than the measured efficiencies of the green EL in out-diffused diodes.

The green EL at room temperature is probably extrinsic in origin but further work is clearly necessary on this point.

E. Infrared Band

The infrared band or bands near 1.3 eV in the EL spectra have as yet not been correlated with any PL bands. There may in fact be different infrared bands in different diodes since unintentional dopants or defects are involved. Time decay measurements suggest that the infrared EL may also be a donor-acceptor pair

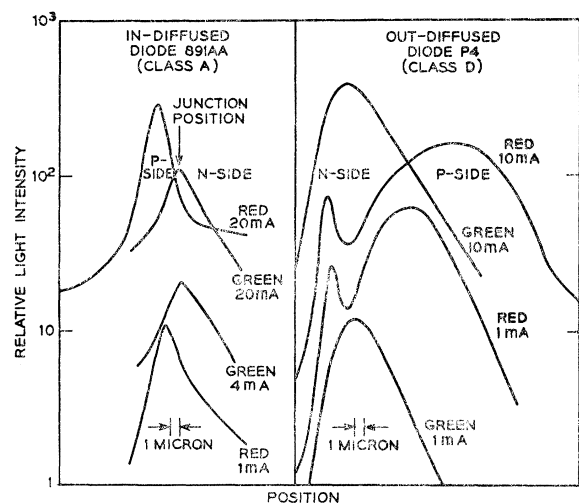


FIG. 10. The emission intensity versus the position perpendicular to the junction plane along a cleaved surface for both an in-diffused and out-diffused diode. The junction position as determined from the electro-optic effect (Ref. 32) is shown for the in-diffused diode.

transition involving at least one deep level. Its decay was studied at several temperatures between 200 and 300°K. The decay, shown in Fig. 9, is nonexponential in time and at long decay times approximates a t^{-2} dependence on time at the lowest temperature. Such a bimolecular-like decay is expected for a pair band at temperatures where some thermal ionization and re-trapping of trapped carriers is possible.³¹ At higher temperatures a decay faster than t^{-2} is expected.

V. INJECTION-RECOMBINATION KINETICS

A. Spatial Distribution

The spatial distributions of the red and green EL light emerging from the cleaved faces of several of the more efficient diodes have been examined. The image formed by a microscope, of a cleaved face perpendicular to the junction plane, was scanned with a photomultiplier tube having on it a slit and appropriate filters. Since the diode thickness is large compared with the depth of field of the microscope, some blurring of the spatial distribution of emission occurs. Define a quantity h as the maximum distance from the junction plane that a ray of light, emitted at the junction at the bottom surface of the diode, can strike the top surface of the diode and still enter the microscope objective. If l is the top-to-bottom length of the diode, n the index of refraction, and Γ the numerical aperture of the objective, then $h = l\Gamma(n^2 - \Gamma^2)^{-1/2}$. If w is a typical width of the light emitting region, then significant blurring will occur when $w < h$. For the in-diffused diodes $h \approx 50 \mu$ while for the smaller out-diffused diodes $h \approx 10 \mu$ ($\Gamma = 0.34$, $n = 3.3$). Since w is expected to be a

few microns at most for both types of diodes, considerable blurring will occur. When $w \ll h$, the experimentally measured light distributions of a saturated, expanding EL layer will grow in peak height and shift in peak position. As w approaches h , saturation will appear on the side of the experimental distribution next to the junction but not on the other side, while the shift of the peak will continue. Thus a comparison of the measurements at different currents (and different colors) can be used to establish the saturation of the EL layer.

Figure 10 shows such distributions for red and green EL at two current values for both an in-diffused and an out-diffused diode. The weakness of the infrared EL prevented similar measurements for it. For the in-diffused diode the junction position (marked by an arrow) was determined in the same microscope set-up by observing the position of the electro-optic effect of the junction electric field.³² Such a measurement was not possible on the out-diffused diodes apparently owing to the closeness of the junction to the surface and to a greater optical nonuniformity in the junction region.

Figure 10 shows that the maximum of the green EL from the in-diffused diodes is located at the center of the junction and is stationary as the current is changed while the red EL is located on the p side and moves further into the p side at the higher current. Since $w \ll h$, these observations are consistent with a red EL region saturated in brightness but expanding in width from the edge of the space-charge region further into the p side with increasing applied potential. From these facts we conclude three things about this diode: (1) the green EL is generated predominantly in or near the space-charge region; (2) the red EL is emitted from a saturated region on the p side which expands with increasing bias; (3) the expansion of the red EL region (enlarging diffusion length) means that all significant radiative and nonradiative recombination mechanisms are saturated on the p side.

The green EL from the out-diffused diode of Fig. 10 has a similar distribution to that from the in-diffused diode and is also stationary with changing current. It is thus reasonable to assume the junction to occur where the green EL maximum occurs (which is about 4μ in from the surface). This falls at a minimum in the red EL distribution, there being peaks on both the n and p sides. The absence of a green EL peak on the n side like that of the red EL leads us to conclude that the peak is not an artifact of the optical geometry but is rather a real emission peak. The dominant red EL is still from the p side, and its peak is seen to move about 6μ farther into the p side as the current is increased from 1 mA to 10 mA. Note that there is little increase in the red EL with current near the junction but a substantial increase far away from it. From this diode two more conclusions can be drawn: (1) while the red

³¹ D. G. Thomas, J. J. Hopfield, and W. M. Augustyniak, Phys. Rev. **140**, A202 (1965).

³² D. F. Nelson and F. K. Reinhart, Appl. Phys. Letters **5**, 148 (1964).

EL can be generated on both the n and p side it is strongest on the p side; (2) generation of red EL per unit volume is much less in the space-charge layer than outside it.

Figure 11 shows the spatial distributions of red and green EL from a more efficient out-diffused diode of broader area at several current values. Figure 12 shows a composite photograph of the red and green EL of this diode. The EL distributions shown in Fig. 11 begin at lower current densities than those of Fig. 10. The red EL distributions show a greater saturation near the junction at higher currents as expected when w approaches h . The red peak is also seen to move farther into the p side as for the diodes of Fig. 10. Considerably greater structure is seen in the green EL distributions than in those of Fig. 10. In this diode the main green EL occurs on the p side at low currents with only small contributions from the space-charge region and the n side. The space-charge region, however, soon becomes the dominant EL location with the resultant spatial distribution approaching the shape seen in the other diodes. Therefore, the green EL can be generated on both the n and p sides but at moderate to high biases it is most efficiently generated in the space-charge region of the out-diffused diodes.

In summary, the red EL is generated predominantly on the p side of the junction in all diodes studied, it saturates in its brightness, and the red emitting region then expands in width. The green EL is generated predominantly in the space-charge layer in out-diffused diodes at moderate-to-high biases; in in-diffused diodes, the situation appears the same but significant green EL from nearby n and p material cannot be excluded.

An accompanying paper⁷ predicts the saturation of the red EL in a layer adjacent to the space-charge layer and the expansion of this layer with increasing current.

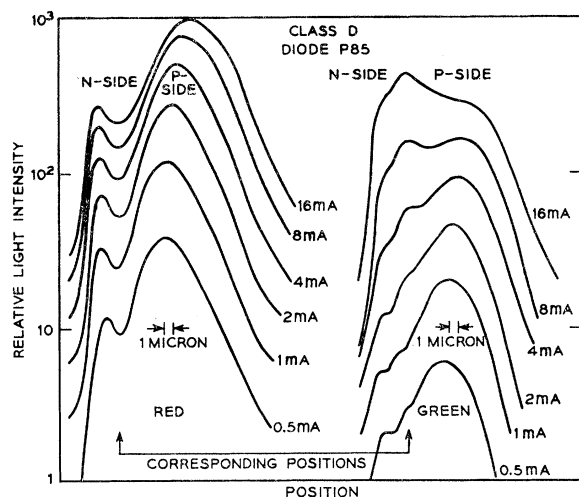


FIG. 11. Emission intensity versus position (as in Fig. 10) for an out-diffused diode. Note the saturation of the red EL near the junction, the motion of the red peak farther into the p side, and the growth of the green EL from the space-charge layer.

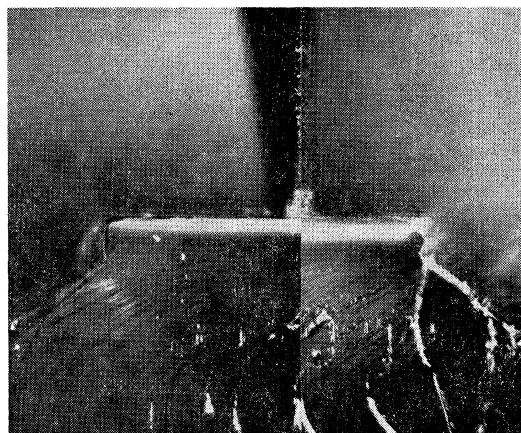


FIG. 12. The cleaved edge of the class-D diode of Fig. 11 made by out-diffusion of Zn for 5 h at 600°C from a compensated crystal (grown from a melt containing 0.05 atom % Zn, 0.01% Te and 0.01% Ga₂O₃). The photograph was obtained with both EL (10 mA) and ambient light, the left and right side portions viewed through green and red filters, respectively. The spatial separation of the red and green EL components is apparent. The lateral dimension of the junction is 0.25 mm.

The spatial distribution measurements are consistent with these predictions, since $w \ll h$. Further discussion of these distributions will be deferred until the next section.

B. Steady State

In the following experiments, in which the EL intensity for each of the three peaks was measured as a function of current and voltage, the dc and pulsing techniques previously described were used but appropriate filters were substituted for the monochromators. The pulse length was adjusted (0.5 to 50 μ sec) so that steady state was reached before the end of the pulse.

In the last section it was shown that the red EL was generated on the p side beyond the space-charge layer, while the green EL came from in or near the space-charge layer at moderate bias levels. It was previously shown from the electrical properties that the total junction current was a sum of independent parallel currents, each driven by the applied junction bias. Since the dominant junction current has already been shown to arise from recombination within the space-charge layer, usually at deep levels, it is clear that the fundamental kinetic relationships governing the light generation processes relate light emission to applied potential, not to current.

To emphasize this point, we plot in Fig. 13 the intensity of each EL peak (red, green, and infrared) for a class-C diode versus the total current on a log-log scale. Since, as we have already seen, the dominant space-charge layer current can be represented by $\exp(qV/nkT)$ where n changes rather abruptly in different bias regions, the EL intensity for each peak must depend upon current as $L \propto I^n$ with n changing rather abruptly between regions as Fig. 13 shows. The intensity of each

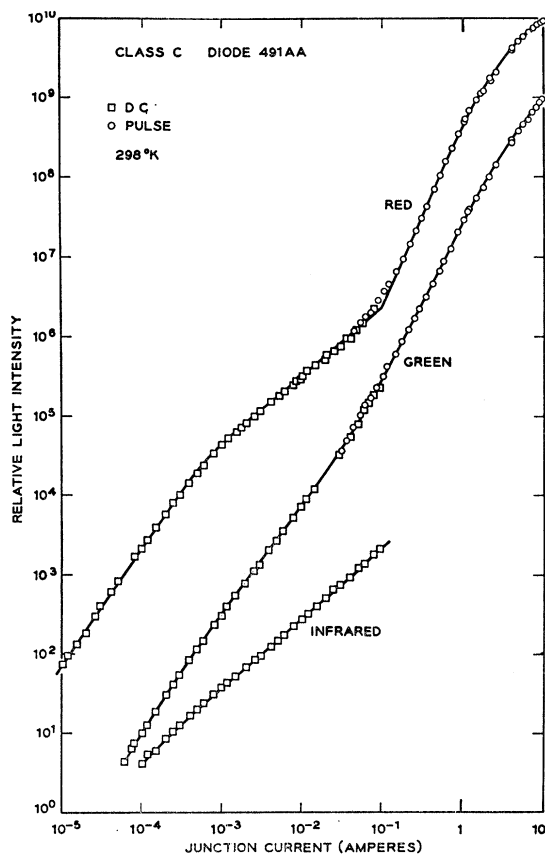


FIG. 13. The intensities of the red, green, and infrared EL bands versus forward bias current for the class-C diode whose electrical properties were examined in Sec. IIIC. The three curves are not normalized to each other.

EL peak for this diode is plotted in Fig. 14(a) versus the applied potential, the latter on a linear scale. At low bias and room temperature the red and green emission bands vary with bias as $\exp(qV/mkT)$, with $m=1.00 \pm 0.03$. In this diode the low bias region ($m=1$) is not reached for the infrared EL. In some diodes, however, an $m=1$ region is seen in the infrared EL at the lowest biases. Figure 14(b) shows similar behavior for a class-B diode.

We next show that each EL band intensity varies as $\exp(qV/kT)$ at low bias for a wide range of temperatures. In Fig. 15 the intensity of the red EL band in the out-diffused diode whose current-voltage characteristics were shown in Fig. 3 is plotted logarithmically against bias at a number of temperatures. The solid lines are drawn with slope q/kT . Such data are typical of in-diffused and out-diffused (Zn or Cd) diodes and for each EL band.

At high bias some of the curvature in the EL intensity-versus-bias plots (Figs. 14 and 15) can be eliminated by invoking the series resistance drop, the later derived from the $I-V$ curves. When this is done, (see Fig. 14), it is apparent that the green emission varies as $\exp(qV/kT)$ to the highest deduced potentials

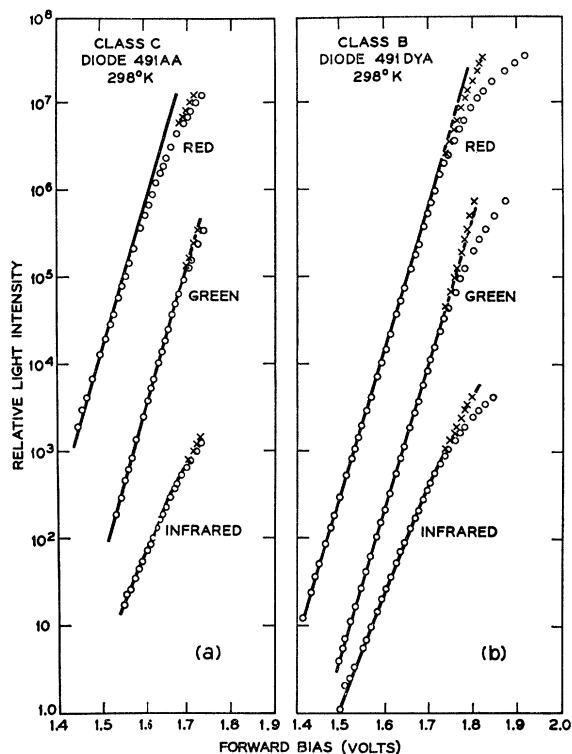


FIG. 14. The unnormalized intensities of the red, green, and infrared bands as a function of forward bias for a class-C and a class-B diode. The crosses indicate series resistance corrections to the bias. The straight lines drawn through the red and green data have a slope of q/kT .

(~ 1.85 V). However, the red EL begins varying less rapidly than this at high bias even below the region where the correction for series resistance is important. It varies as $\exp(qV/mkT)$, where $m=1$ at low bias and

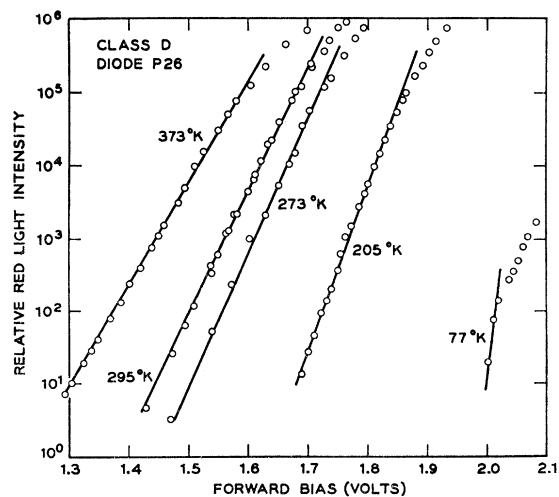
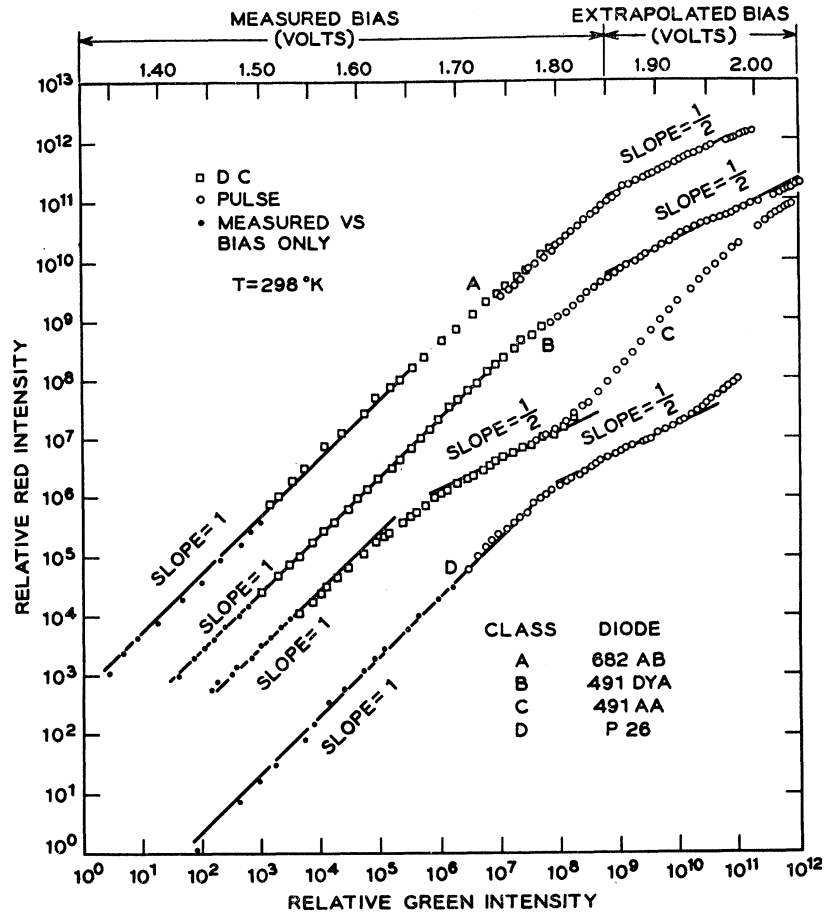


FIG. 15. The relative intensity of the red emission from a class-D diode as a function of bias at several temperatures. No series-resistance corrections are made and the straight lines are drawn with a slope of q/kT at each temperature. The $I-V$ characteristics for this diode were shown in Fig. 3.

FIG. 16. The red EL intensity for a diode from each class versus the green EL intensity on a log-log scale. The four curves are not normalized to each other. The junction bias which is proportional to the logarithm of the green emission is shown on the linear scale above the graph. At low to moderate biases it is measured directly, while at high bias it is assumed proportional to the logarithm of the green intensity. The dots at the lowest biases are measured as a function of bias only since the green intensity is too weak to measure there. The linear and half-power regions are indicated.



approaches 2 at high bias. The infrared behaves qualitatively the same except that the $m=1$ region is often below the range of measurement.

We will assume that the green emission varies as $\exp(qV/kT)$ even beyond the region where V can be measured. This can be justified as follows. At high bias the green EL is generated within the space-charge layer, as shown previously, so that the SNS recombination theory must be used. Since the EL peak lies extremely close to the band gap, the center responsible for the emission must lie very close to either the conduction band or the valence band. Thus in Eqs. (4) and (5) $|2(E-E_i)|$ must be very close to V_d . From Eq. (5), V can never exceed V_k . Therefore, Eq. (4) is the applicable SNS form, with $|2(E-E_i)| \sim V_d$. The term in the brackets in Eq. (4) becomes $V_d - V$ provided $V_d - V \gg kT$, thereby cancelling the same term in the denominator. Thus, the green EL depends upon $\exp(qV/kT)$, with all pre-exponential dependence on V removed except the weak dependence contained in W . If any green EL is generated on the n side, it would depend on $\exp(qV/kT)$ alone.¹⁸ In contrast to the space-charge recombination from deeper levels which gives rise to the dominant current, the green EL provides a simple measure of the true junction bias even at biases where series

resistance corrections preclude direct measurements of the bias. In fact, comparison of green EL versus voltage data with $I-V$ characteristics can be used to indicate

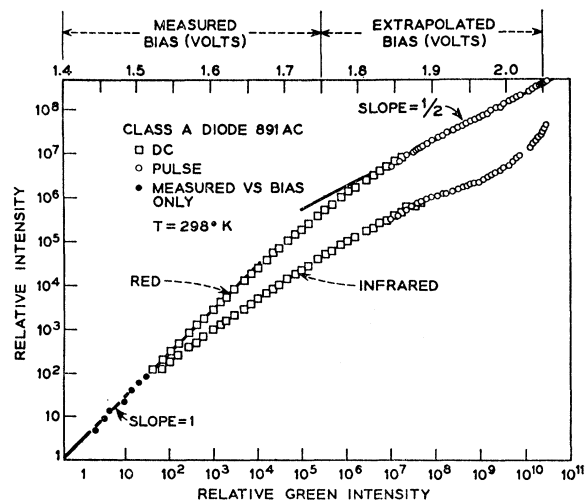


FIG. 17. The intensities of both the red band and the infrared band versus the green intensity for a class-A diode on a log-log scale. The two curves are not normalized to each other. See Fig. 16 for a description of the upper bias scale. The linear and half-power regions for the red band are shown.

when series resistance corrections to the bias become necessary.

The intensity of the red EL is plotted against the green EL intensity for the representative diodes of each class on a log-log scale in Fig. 16. Similar data for both red and infrared EL for a class-A diode are shown in Fig. 17. The abscissa is linear in bias and this voltage scale also is shown and extrapolated into the region where V can no longer be directly measured.

For all diodes studied the intensity of the red EL, R , depends on bias as $\exp(qV/kT)$ for biases $\ll 1.8$ V, that is, $\ln R$ has a unit slope when plotted versus qV/kT (see Fig. 16). After a transition region usually near 1.8 V a region of slope $\frac{1}{2}$ occurred for all diodes studied regardless of the level of O doping. In many diodes this dependence persists to the highest biases studied. In other diodes a third region at higher bias is observed where $\ln R$ versus qV/kT has a slope larger than $\frac{1}{2}$. In several diodes like the class-D diode shown, the slope has returned to about 1 at the highest biases obtained. In the class-C diodes, this third region is very extended and a slope slightly greater than one (1.2) is reached before the slope again becomes sublinear.

These dependences can be understood on the basis of the accompanying paper.⁷ It predicts four regions, each having a constant slope of $\ln R$ versus qV/kT , for the EL emitted in the carrier diffusion region (beyond the space-charge layer) of a junction from a level deep in the forbidden gap. The first predicted region (simple linear recombination) has a slope of 1 as observed. After a transition region a second region of slope $\frac{1}{2}$ is predicted. This region corresponds to the saturation of the red center population (and also the dominant recombination center population) in a volume close to the space-charge layer. Within this volume the EL brightness would be constant. The sublinear rise in the red EL intensity in the slope $\frac{1}{2}$ region is due to the expansion of this saturated volume. The red EL spatial distributions (Figs. 10 and 11) that show an expansion of the EL volume were measured at biases in the slope $\frac{1}{2}$ region. Thus the spatial distributions give strong support to the proposed explanation for the $\ln R$ versus qV/kT curves.

The voltage in the center of the transition region between the slope 1 and the slope $\frac{1}{2}$ regions can be expressed as⁷

$$eV_{12} = kT \ln M p_0^2 / n_1^2 A, \quad (9)$$

where $A/M = p_0/n_1$ when the thermal ionization rate from the donor is faster than the donor-acceptor pair recombination (n_1 is the density of free electrons when the Fermi level is at the donor level). This is true for Zn-O pair recombination in p -type GaP at 298°K.¹⁸ An average value of V_{12} found from many diodes is 1.76 ± 0.05 eV. With $n_1 = 2 \times 10^{12}$ cm⁻³ corresponding to the O center being at 0.4 eV below the conduction band, we find $p_0 = 2 \times 10^{18}$ cm⁻³, a very reasonable value.

A third region is predicted⁷ to occur when the drift term in the continuity equation becomes comparable to the diffusion term. In this region the slope of $\ln R$ versus qV/kT is predicted to be $(n+1)/n$ where n is defined by the I - V characteristic [$I = I_0 \exp(eV/nkT)$]. At this bias the dominant current can be a combination of diffusion-region and space-charge-layer recombination. The upper experimental region, particularly evident in class-C diodes, is believed due to this cause even though the experimental slope (1.2) never reaches 1.5, the value expected for $(n+1)/n$ on the basis of Fig. 19. This may be attributable to the shortness of this region experimentally, that is, the transition to the next higher region occurring before the approximations needed for the $(n+1)/n$ slope prediction become sufficiently valid.

The theory also predicts a fourth region where $\ln R$ versus qV/kT again has a slope of $\frac{1}{2}$. This occurs under strong conductivity modulation, that is, for an injected minority carrier density greater than the equilibrium majority carrier density. Transition to this region would occur at a voltage determined by $np = n_i^2 \exp(qV_c/kT)$, with $n = p$. For GaP at room temperature, $n_i \approx 1.4$ cm⁻³ and so for $p = 10^{18}$ cm⁻³, $V_c = 2.09$ V. This upper $\frac{1}{2}$ power region will occur for $V > V_c$ which is a junction voltage greater than any reached in these measurements.

The voltage dependence of the intensity, F , of the infrared EL is qualitatively similar to that of the red EL. At very low biases $\ln F$ versus eV/kT has a unit slope. This has been observed in only the few diodes which have strong infrared EL at the very low biases. A slope of $\frac{1}{2}$ for $\ln F$ versus eV/kT is then observed in some diodes, though in others (see Figs. 14 and 17) only an extended sublinear region is seen. At high biases a return of the slope back to near unity occurs. Though the sublinear region can sometimes be fit quite well by the SNS theory (space-charge-layer recombination), the presence of the high bias up-turn (see Fig. 17) suggests the effects of drift on the recombination process in a carrier diffusion region.

The infrared EL arises from an unintentionally added and unidentified center (or centers). It is too weak for spatial distribution measurements to be made and often too weak for its spectrum to be measured (though with filters its voltage dependence can be determined). Thus we do not know whether the infrared EL arises from the n side, the p side, the space-charge layer or a combination of these locations. Neither are we sure that we are dealing with one rather than several infrared bands at different wavelengths. For these reasons we will not attempt to account theoretically for the infrared curves of Figs. 14 and 17.

C. Transient Effects

In about one-half of the diodes that have been studied in the pulse range of excitation a risetime of the red EL has been observed at room temperature. This risetime shortens with increasing pulse current. No

TABLE II. External efficiencies of the red EL in representative (but not the best) diodes from each class. L_0 is defined by Eq. 11. p_0 is the majority carrier density derived from these data with $\tau_R=9\times 10^{-8}$ sec for all diodes (τ_R and τ_m are defined in the text.)

Class	Diode	L_0 (photons/sec cm ²)	τ_m (sec)	p_0 (cm ⁻³)	External quantum efficiency	Current density (A/cm ²)
A	682AB	28×10^{-15}	1.5×10^{-9}	4.2×10^{16}	1.0×10^{-4}	3.3
B	491DVA	3.6×10^{-15}	2.5×10^{-8}	1.3×10^{18}	3.5×10^{-5}	3.4
C	491AA	0.28×10^{-15}	7.0×10^{-10}	2.7×10^{18}	2.7×10^{-7}	4.2
D	P26	58×10^{-15}	2.7×10^{-9}	2.7×10^{16}	1.3×10^{-4}	10

corresponding decay of the red light is observed. Neither is there any risetime or decay time of the green EL observed which is longer than 10 nsec, the instrumental risetime.

These observations have the characteristics not of a process intrinsic to the red EL, but of the filling of a saturable trap on the *p* side of the junction where the red EL emission mostly occurs. Such a trap filling would not affect the green EL which is generated predominantly in the space-charge layer.

One diode exhibiting these transient effects (a class-B diode: 493AC) was chosen for careful study. The current pulses were supplied by a Spencer-Kennedy Laboratories model 503A fast rise pulse generator. The EL was detected by an RCA 7326 photomultiplier with appropriate filters. Its signal was fed into a Hewlett-Packard 185B sampling oscilloscope and its output plotted on an *x-y* recorder. The exponential risetime as deduced from these observations is plotted in Fig. 18 versus the junction current. It is seen to decrease as the inverse half power of the current. We will not attempt an analytical treatment of this decay as it would require solution of the time-dependent diffusion equation coupled to the nonlinear (because of saturation) time-dependent trap population equation—a formidable task.

Further evidence in support of this model comes from the observation that in the current range studied a broad, rather strong near-infrared EL ($h\nu\approx 1.3$ eV) is rapidly saturating. The center generating this EL is probably the trap (a deep donor) which is being filled. From the decay of the infrared EL in this diode, as shown in Fig. 9, it may also be a donor-acceptor pair recombination process.

D. Radiative Efficiency

The relative efficiencies of all three EL bands are indicated in Fig. 6. Here we shall consider the dominant red EL only. We have already shown that the EL and the junction current derive from essentially independent mechanisms. Thus quantum efficiencies which depend on the total junction current will have less significance than an efficiency which depends on the bias. At low bias (<1.65 V) injection and radiative recombination on the *p* side are linear processes. The current density

due to injection of minority carriers is

$$J_D = (qn_i^2 D_n^{1/2} / p_0 \tau_n^{1/2}) \exp(qV/kT), \quad (10)$$

where D_n is the diffusion constant of electrons, p_0 the equilibrium free-hole concentration and τ_n the minority carrier lifetime.¹³ The radiative recombination rate is

$$L = (\tau_n / \tau_R) J_D = L_0 \exp(qV/kT), \quad (11)$$

where τ_R is the minority carrier lifetime if only the radiative center were present and $L_0 = qn_i^2 (D_n \tau_n)^{1/2} / p_0 \tau_R$.

Table II lists, for a typical example of each diode class, the measured values of τ_m (see Sec. IIIB) and L_0 with no corrections for self absorption. The red EL of the class-D diodes arises from injection into the homogeneous *p*-side material where PL measurements indicate a typical quantum efficiency (τ_n / τ_R) of $\sim 3\%$. Assuming $\tau_m = \tau_n$ ($= 2.7 \times 10^{-9}$ sec from Table II) one may estimate $\tau_R = 9 \times 10^{-8}$ sec for the class-D diode. It is reasonable to assume τ_R to have this value for all diodes and for the efficiencies to vary through changes in τ_n . The value of p_0 listed in Table II is that deduced using this assumption and the measured values of L_0 and τ_m , and it is to be noted that the value of p_0 so obtained increases with increasing diffusion temperature, a result which could reasonably be expected. For a constant diffusion temperature (p_0 constant) the efficiencies scaled with τ_m .¹⁴

The dominant current at low bias is due to space-charge recombination at deep levels with the current varying with bias as $\exp(qV/2kT)$ and somewhat more

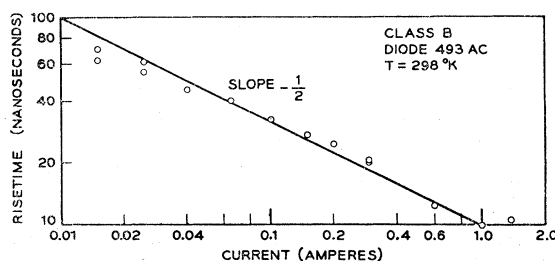


FIG. 18. The exponential risetime of the red EL versus current. The effect is attributed to the filling of a deep trap as discussed in the text.

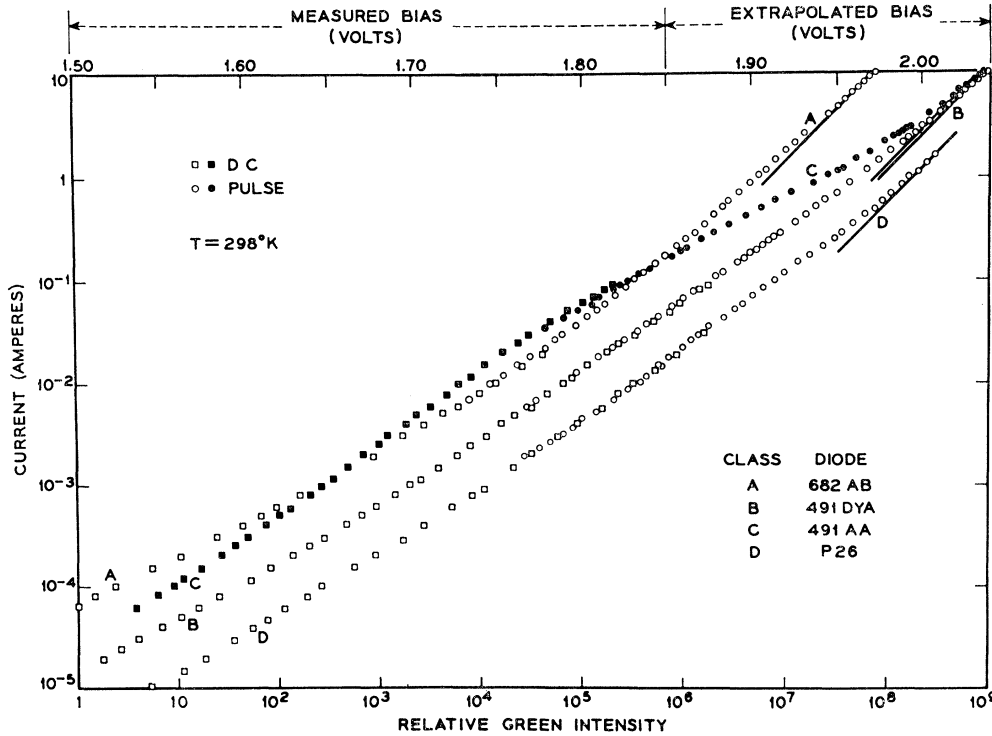


FIG. 19. The total junction current for a diode from each class versus the green EL intensity on a log-log scale. The upper bias scale is derived in the same way as in Fig. 16. The straight lines drawn at the highest biases correspond to $I \propto \exp qV/kT$.

rapidly as the bias approached V_d . (In the class-C diodes shallow-level space-charge layer recombination begins to dominate at medium to high bias. Here the current varies as $\exp(qV/nkT)$, with $n < 2$.) The red EL varies in intensity as $\exp(qV/mkT)$, with $m = 1$ at low bias and slowly increases to 2 in the saturation region. Hence the quantum efficiency of the red EL increases with bias as $\exp(qV/2kT)$ at low bias where the EL involves linear recombination and the competing current process is due to simple deep-level space-charge-layer recombination. This is true of all the diodes.

Above ~ 1.8 V, where the I - V curves can no longer be measured directly, the green EL may be used to indicate the true junction bias (see Sec. VB). In Fig. 19 the total junction current is plotted against the green EL on a log-log graph for the typical diodes of each class. The logarithmic abscissa is converted to a linear bias scale, as described in Sec. VB, and is also shown in Fig. 19. Above 1.85–2.00 V, I approaches $\exp qV/kT$ in each case. This should be due to diffusion current (see Sec. IIIA). From Sec. VB, the recombination centers on the p side are saturated at these biases and as a result the current injected into the p side varies as $\exp(qV/2kT)$.⁷ Therefore the dominant current at high bias deduced from Fig. 19 must be due to n -side injection. Thus the dominant recombination centers on the p side are saturated at these high biases, while those on the n side are not. If these centers are the same on

both sides of the junction, they must be acceptor-like in character ($\tau_n/\tau_p \gg 1$).

Since at high bias the red EL is in the saturation regime ($\propto \exp(qV/2kT)$) and the dominant current is due to n -side injection ($\propto \exp(qV/kT)$), the quantum efficiency must decrease as $\exp(-qV/kT)$ in this bias range. Thus the quantum efficiency should exhibit a maximum at ~ 1.8 V, which is in fact observed.

It is worth noting that saturation of the recombination centers on the p side implies that the centers within the space-charge layer are always filled with electrons, since the free-electron concentration in the space-charge layer is always greater than that on the p side and the free-hole concentration is always less. Thus the p -side injection current must be greater than the space-charge current in this range. This assumes that the dominant recombination centers are the same in both regions.

The measured external quantum efficiencies are also listed in Table II for the representatives of each diode class along with the corresponding current densities. These efficiencies are not corrected for self-absorption. Note that these efficiencies parallel the corresponding values for L_0 . This is because the dominant deep-level space-charge current density is the same (within a factor of five) for all the diodes. The most efficient diode classes are A and D with quantum efficiencies ranging up to 2×10^{-3} in class-A and up to 7×10^{-3} in class-D diodes.

Note added in manuscript: In diodes prepared by growing an n -type Te-doped layer epitaxially from solution onto a p -type seed doped with Zn and O [M. R. Lorenz and M. P. Pilkuhn, Extended Abstracts, Electronics Division, Electrochem. Soc. **14**, 79 (1965)], the dominant emission is also the Zn-O red band discussed here. We have found that this red EL also shifts spatially and varies with bias like the diodes of Fig. 16.

ACKNOWLEDGMENTS

We are indebted to F. A. Trumbore and M. Kowalchik for growing the crystals used here, to E. Dickten for developing the junction fabrication techniques, to R. M. Mikulyak, K. F. Rodgers, and H. G. White for assistance with the measurements, and to D. A. Kleinman, D. G. Thomas and C. D. Thurmond for many useful discussions.

Crystal Potential and Correlation for Energy Bands in Valence Semiconductors*

WILLIAM BRINKMAN† AND BERNARD GOODMAN‡

University of Missouri, Columbia, Missouri

(Received 3 March 1966; revised manuscript received 11 May 1966)

A number of forms of the one-electron potential for a semiconductor are evaluated on the basis of orthogonalized-plane-wave (OPW) calculations for Si. Starting with the Hartree-Fock (HF) equations, a method of calculating the exact core exchange is developed and various approximations to the valence exchange are considered. Some of these approximations are considered only to illustrate the effect of certain features on the energy bands. None contain adjustable parameters. The $\mathbf{k}\cdot\mathbf{p}$ method in conjunction with *a priori* calculations at $\mathbf{k}=0$ is proposed as a convergent method for obtaining the energy bands throughout the zone and for achieving self-consistency. The procedure is quite simple if the potential is local. A completely self-consistent calculation is carried out using the Slater approximation to the valence exchange. Although agreement with experiment is reasonable, the differences are such that they cannot be attributed to computational errors. Following the procedure of Kleinman and Phillips the HF valence-exchange matrix elements were estimated from an 8-point sampling of the Brillouin zone. The calculated energy differences between the conduction and valence bands at symmetry points are much larger than the measured values, so that an effective potential including correlations is necessary. Correlations are included in generalized OPW equations. Because the core exchange is essentially unscreened, the core states for orthogonalization are still of the HF type. A nondiagonal self-energy operator is derived on the basis of a Coulomb-hole-plus-screened-exchange approximation suggested by Hedin. Calculations are performed at symmetry points using simplifications of this self-energy in which the nondiagonal components of the dielectric function are neglected. The results are not an improvement over the Slater approximation.

I. INTRODUCTION

CONSIDERABLE success in correlating electronic properties of solids has been achieved by the use of calculations which are more or less explicitly parameterized and adjusted to fit some observations. A recent example is the use of the pseudopotential^{1,2} introduced by Phillips.³ These methods exploit certain features of the electronic states without attempting to give accurate solutions of the Schrödinger equation. An understanding of the values and significance of the parameters themselves as well as numerous quantitative

features will have to be obtained from first-principle calculations.

Operationally, the problems of performing such calculations may be separated into those of reducing the N -particle equation to a tractable form and those of developing convergent numerical procedures for solving the simplified equations as well as for calculating physical quantities such as charge densities and optical transition probabilities. The present work attempts to make some progress in both respects, developing procedures to facilitate attaining self-consistency in energy band calculations and also presenting calculations based on several reasonable forms of the effective one-electron wave equation. The work is carried out using the orthogonalized-plane-wave (OPW) formalism.

Considerations are limited to semiconductors and the numerical calculations were done for silicon for which several other calculations are available for com-

* Based on work submitted in partial fulfillment of the requirements for the degree of Doctor of Philosophy from the University of Missouri by William Brinkman.

† Present address: Bell Telephone Laboratories, Murray Hill, New Jersey.

‡ Present address: University of Cincinnati, Cincinnati, Ohio.

¹ W. Harrison, Phys. Rev. **129**, 2503 (1963); **129**, 2512 (1963); **131**, 2433 (1963).

² D. Brust, Phys. Rev. **134**, A1337 (1964).

³ J. C. Phillips, Phys. Rev. **112**, 685 (1958).

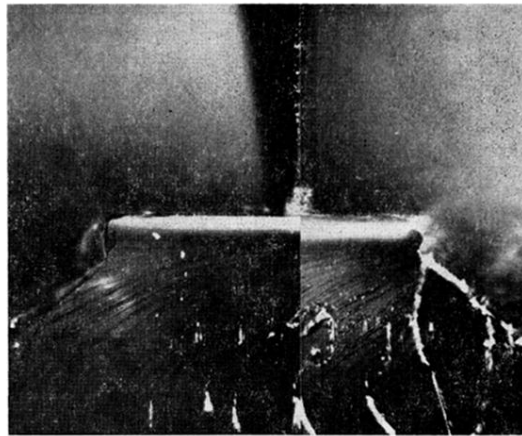


FIG. 12. The cleaved edge of the class-D diode of Fig. 11 made by out-diffusion of Zn for 5 h at 600°C from a compensated crystal (grown from a melt containing 0.05 atom % Zn, 0.01% Te and 0.01% Ga₂O₃). The photograph was obtained with both EL (10 mA) and ambient light, the left and right side portions viewed through green and red filters, respectively. The spatial separation of the red and green EL components is apparent. The lateral dimension of the junction is 0.25 mm.